

Article

Intrinsic Thermal Stability of Li-Rich Mn-Based Cathodes Enabling Safe High-Energy Lithium-Ion Batteries

Zhaoqiang Pei ^{1,2}, Shaobo Feng ^{1,2}, Zhibo Han ³, Zihua Wang ³, Chengshan Xu ^{1,2}, Xiangming He ⁴ , Li Wang ^{4,*} , Yu Wang ^{1,2,5,*}  and Xuning Feng ^{1,2} 

¹ School of Vehicle and Mobility, Tsinghua University, Beijing 100084, China; zy2243502@buaa.edu.cn (Z.P.); fsb22@mails.tsinghua.edu.cn (S.F.); xcs_pcg@mail.tsinghua.edu.cn (C.X.); fxn17@tsinghua.edu.cn (X.F.)

² State Key Laboratory of Intelligent Green Vehicle and Mobility, Tsinghua University, Beijing 100084, China

³ School of Material Science and Engineering, Beihang University, Xueyuan Road, Beijing 100191, China; 20375387@buaa.edu.cn (Z.H.); sy2343112@buaa.edu.cn (Z.W.)

⁴ Institute of Nuclear and New Energy Technology, Tsinghua University, Beijing 100084, China; hexm@tsinghua.edu.cn

⁵ Center for Combustion Energy, Tsinghua University, Beijing 100084, China

* Correspondence: wang-l@tsinghua.edu.cn (L.W.); lucywang@mail.tsinghua.edu.cn (Y.W.)

Abstract

Lithium-rich manganese-based oxides (LMR) are promising next-generation cathode materials due to their high capacity and low cost, but safety remains a critical bottleneck restricting the practical application of high-energy-density cathodes. However, the safety level of LMR batteries and the thermal failure mechanism of the cathode are still poorly understood, especially when compared with traditional high-energy nickel-rich (Ni-rich) cathodes. Here, we investigate the LMR cell's thermal runaway behavior and the thermal failure mechanism of the cathode. Compared to a Ni-rich cell, Accelerating Rate Calorimetry (ARC) shows the LMR pouch cell exhibits a 62.7 °C higher thermal runaway trigger temperature (T₂) and 270.3 °C lower maximum temperature (T₃). These results indicate that the cell utilizing a higher-energy-density LMR cathode presents significantly lower thermal runaway risks and hazards. The results of differential scanning calorimetry–thermogravimetry–mass spectrometry (DSC-TG-MS) and in situ heating X-ray diffraction (XRD) indicate that the LMR cathode has superior thermal stability compared with the Ni-rich cathode, with cathode oxygen released at higher temperatures and lower rates, which is beneficial for delaying and mitigating the exothermic reaction inside the battery. This study demonstrates that simultaneously enhancing cathode energy density and battery safety is achievable, and these findings provide theoretical guidance for the design of next-generation high-energy and high-safety battery systems.

Keywords: battery safety; thermal runaway; lithium-rich manganese-based oxides; NCM layered oxides; thermal stability; cathode oxygen release

1. Introduction

The growing demand for high-energy-density lithium-ion batteries (LIBs) in electric vehicles and grid-scale energy storage has driven the development of advanced cathode materials beyond conventional layered oxides [1–3]. Among these, lithium-rich manganese-based oxides (LMRs) deliver capacities exceeding 250 mAh g⁻¹ through anion redox reactions, positioning them as one of the most promising next-generation cathode candidates [4,5]. However, as critical components of battery safety, the application



Academic Editor: Yong-Joon Park

Received: 9 July 2025

Revised: 31 July 2025

Accepted: 11 August 2025

Published: 15 August 2025

Citation: Pei, Z.; Feng, S.; Han, Z.; Wang, Z.; Xu, C.; He, X.; Wang, L.; Wang, Y.; Feng, X. Intrinsic Thermal Stability of Li-Rich Mn-Based Cathodes Enabling Safe High-Energy Lithium-Ion Batteries. *Batteries* **2025**, *11*, 311. <https://doi.org/10.3390/batteries11080311>

Copyright: © 2025 by the authors. Licensee MDPI, Basel, Switzerland. This article is an open access article distributed under the terms and conditions of the Creative Commons Attribution (CC BY) license (<https://creativecommons.org/licenses/by/4.0/>).

of high-energy-density cathodes may induce safety hazards typified by thermal runaway (TR), which constrains the further development and practical application of high-energy cathodes [6–10].

Conventional high-energy Ni-rich NCM layered oxides cathodes ($\text{Ni} \geq 80\%$) enhance energy density but suffer from intrinsic thermal instability and release of reactive oxygen species (O^* , O_2 and so on), which exacerbate self-heating reactions under thermal abuse, ultimately triggering thermal runaway [11–14]. Further increasing Ni content to boost the energy density of NCM cathodes aggravates their thermal degradation, escalating thermal runaway risks [15–17]. Thus, employing Ni-rich cathodes often entails a trade-off between energy density and safety. But emerging LMR cathodes may overcome this trade-off.

Unlike NCM cathodes reliant on Ni-dominated cationic redox, LMR cathodes harness both transition-metal redox and anionic oxygen redox to achieve high specific capacity ($>250 \text{ mAh g}^{-1}$) [18–20]. Moreover, LMR cathodes typically contain $<50\%$ Ni and form composite lattice frameworks (e.g., monoclinic $\text{C}2/\text{m}$ layered phases integrated with Li_2MnO_3 -like domains or spinel components), creating distinct oxygen sublattice configurations compared to NCM cathodes [21,22]. This suggests that LMR cathodes may deviate from the thermal stability trend observed in Ni-rich cathodes—their higher specific capacity and energy density do not necessarily compromise thermal stability or increase thermal runaway risk. However, the safety implications of LMR cathodes remain unclear, and differences in thermal stability and failure mechanisms—particularly phase-structure stability and cathode oxygen release behavior at elevated temperatures—between LMR and Ni-rich cathodes are poorly understood. This knowledge gap severely impedes the rational design of safe, high-energy cathodes.

Therefore, we first employed accelerating rate calorimetry (ARC) to compare the safety of fully charged 1Ah LMR | Graphite and NCM92 | graphite pouch cells, quantifying their thermal runaway risk and hazard. Complementary characterizations, including DSC-TG-MS, in-situ heating XRD, and HRTEM, were used to contrast the thermal stability, phase evolution, and cathode oxygen release behavior of fully charged LMR and NCM92 cathodes. Results demonstrate that cells equipped with higher-specific-capacity/energy LMR cathodes exhibit significantly reduced thermal runaway risks and severity (TR trigger temperature (T_2) increased by 62.7°C , TR maximum temperature (T_3) decreased by 270.3°C). Material-level analyses reveal that LMR cells' superior safety originates from enhanced thermal stability and suppressed cathode oxygen release rate. This allows sufficient oxygen reaction with inactive components, releasing CO_2 (rather than O_2) that migrates to the anode, thereby delaying and mitigating exothermic reactions. Thus, the total heat release of the LMR full cell DSC sample is 31% lower than that of the NCM92 sample. These findings demonstrate that it is possible to simultaneously apply high-energy cathodes and improve battery safety. While currently large-scale commercialized LFP batteries exhibit high safety owing to the excellent thermal stability of LFP cathodes, their low energy density restricts applications in specific scenarios. Our study demonstrates that LMR batteries, featuring both high energy density and high safety, precisely fill this unique market niche. The high thermal stability of the LMR cathode and the altered oxygen release behavior enable LMR batteries to exhibit enhanced safety, which provides a low-risk foundation for upgrading battery systems. This enables improvements in both the driving range of electric vehicles and the capacity of energy storage stations, while simultaneously reducing the burden on cooling systems of electric vehicle battery packs or enhancing the long-term safety of energy storage systems. This study provides new insights and material foundations for developing next-generation lithium-ion battery systems with both high energy density and high safety.

2. Materials and Methods

2.1. Experimental Materials and Battery Sample Preparation

The battery samples used in this study were 1 Ah NCM92|Gr pouch cells and 1 Ah LMR|Gr pouch cells. The dry cells were purchased from Hunan Li-Fun Technology Corporation Limited, Changsha, Hunan, China. The NCM92 cathode was loaded with 95.5% active material, the compaction density of the electrode was 3.3 g/cc, and the thickness of the current collector was 12 μm . The LMR cathode was loaded with 96% active material, the compaction density of the electrode was 3.3 g/cc, and the thickness of the current collector was 12 μm . The anode electrode was loaded with 95.7% graphite anode material, the compaction density was 1.5 g/cc, and the thickness of the current collector was 8 μm . The electrolyte used was a commercial EC-based electrolyte purchased from Suzhou Dodo Chemical Technology Corporation Limited, Suzhou, Jiangsu, China. The specific composition was 1 M LiPF₆ in EC/DMC (volume ratio of 3/7). The electrolyte was injected into the dry cells (3.5 g/Ah) in a glove box. The cells were sealed and left for 48 h to allow the electrolyte to fully wet the cells. Then, the cells after electrolyte injection were formed by cycling with a current of 0.1 C. After the formation cycling, the cells were vacuum-sealed to obtain the finished cells. Before the cell disassembly and thermal safety performance tests, the cells were charged with constant-current and constant-voltage (CC-CV). They were charged to 100% SOC (NCM92 cell charging cut-off voltage is 4.2 V, LMR cell charging cut-off voltage is 4.8 V) with a current of 1/3 C and a cut-off current of 0.05 C. The difference in upper charge voltage limits stems from the operating mechanisms and voltage characteristics of the two cathode materials. The NCM92 cathode relies on Ni-dominated cationic redox reactions, reaching full capacity at ~4.2 V—a widely recognized upper limit in both commercial and academic research to avoid structural degradation. In contrast, the LMR cathode achieves its high specific capacity ($>250 \text{ mAh g}^{-1}$) primarily through anionic redox reactions, which require a higher voltage (~4.8 V) to fully activate Li₂MnO₃-like domains and achieve complete delithiation. This voltage difference is not arbitrarily set but determined by the intrinsic electrochemical properties of each material: failing to charge LMR to 4.8 V would prevent capturing its actual full-capacity state, just as limiting NCM92 to a lower voltage would underestimate its true state of charge (SOC). This approach aligns with standard practices in comparative studies of cathode materials; for instance, when comparing Ni-rich NCM and LFP cathodes, LFP is typically charged to ~3.7 V (its intrinsic full-SOC voltage) rather than the ~4.2 V used for NCM [23].

2.2. Battery Safety Assessment-ARC Test

In the investigation of thermal failure characteristics in full cells, the Accelerating Rate Calorimeter (ARC) (Figure 1) is commonly employed for qualitative and quantitative analyses. Conducted under quasi-adiabatic conditions, ARC tests eliminate heat exchange between the battery and its surroundings, such that the temperature rise rate is solely determined by internal exothermic reactions and the battery's heat capacity. This allows ARC results to characterize the intrinsic safety of battery cells. Additionally, the adiabatic environment enhances the instrument's sensitivity in detecting self-heating induced by internal chemical reactions.

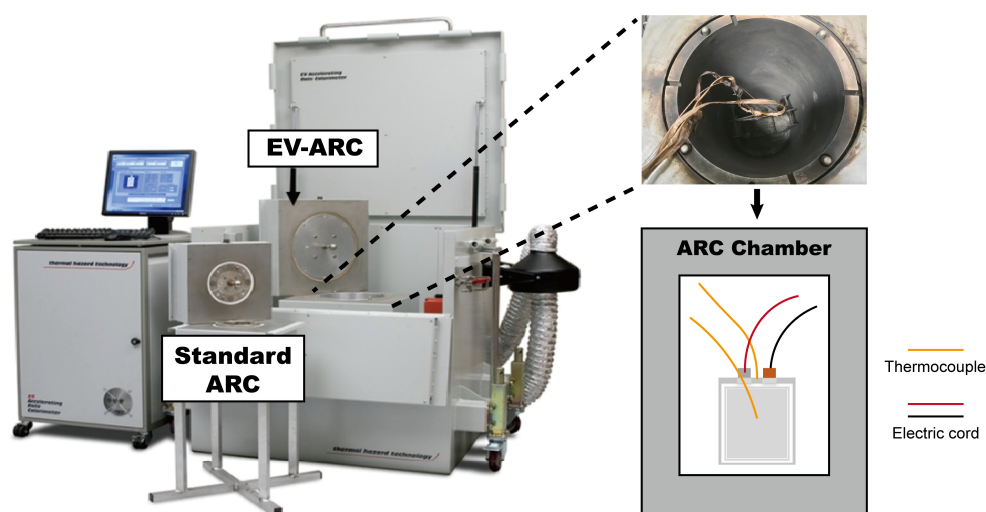


Figure 1. ARC equipment used to evaluate battery safety.

The ARC test in this study was carried out on the Extended Standard ARC (ES-ARC) of Thermal Hazard Technology (THT). Prior to the test, a K-type thermocouple was inserted into the central position inside the fully charged battery to obtain the accurate temperature changes in the battery during the test process. The pouch cells were tested using the Heat-Wait-Seek (HWS) program to acquire the characteristic temperatures that can characterize the battery safety as well as the self-heating rate. The temperature interval was set to 5–10 °C, and the waiting time was set to 20 min. When the battery exhibited self-heating, it entered the adiabatic state to determine the self-heating rate of the battery. If the battery did not experience continuous self-heating when heated to 250 °C, the test was terminated. As shown in Table 1, the temperature at which the battery's temperature rise rate was 0.02 °C/min was defined as the self-heating characteristic temperature T1, and the temperature at which the temperature rise rate was 1 °C/s was the thermal runaway triggering temperature T2 (which means the battery will undergo uncontrolled continuous heat release until it reaches the maximum temperature). The maximum temperature reached by the battery after thermal runaway was T3. These three characteristic temperatures are the key indicators for evaluating battery safety that need to be obtained by ARC test. Generally speaking, the higher the T1 and T2 of the battery in the ARC test, the lower the T3, the lower the risk and harm of thermal runaway of the battery, and the better the safety.

Table 1. Physical meaning and judgment criteria of characteristic temperature obtained by ARC test.

Characteristic Temperature	Physical Meaning	Criteria
T1	The starting temperature of the battery's continuous self-heating	$dT/dt = 0.02 \text{ } ^\circ\text{C}/\text{min}$
T2	Battery thermal runaway trigger temperature	$dT/dt = 1 \text{ } ^\circ\text{C}/\text{s}$
T3	Maximum temperature of battery thermal runaway	/

2.3. Material Level Thermal Failure Analysis Test—DSC-TG-MS

To analyze the thermal stability and exothermic behavior of fully charged electrode materials at the material level, 100% SOC pouch cells were disassembled to obtain electrode materials, with detailed procedures shown in Figure 2. First, the cells were charged to 100% SOC and then transferred into an inert gas-filled glove box ($\text{H}_2\text{O} < 0.01 \text{ ppm}$, $\text{O}_2 < 0.01 \text{ ppm}$). Under inert atmosphere protection, the aluminum–plastic film packaging of the cells was cut open using ceramic scissors. Anode/cathode electrodes and separators were separated using ceramic tweezers. The electrodes were cut to appropriate sizes and

soaked in excess DMC solvent for 1 h, respectively. After rinsing with DMC, the electrodes were soaked again in fresh DMC for another hour to thoroughly remove residual electrolyte and lithium salts. The washed electrodes were first dried in the glove box for 1 h, and then transferred to the glove box's transition chamber for vacuum drying. Subsequently, electrode material powders were gently scraped from the central area of the dried electrodes using a ceramic blade inside the glove box and stored in sealed tubes. This completed the disassembly of cells and preparation of fully charged electrode materials.

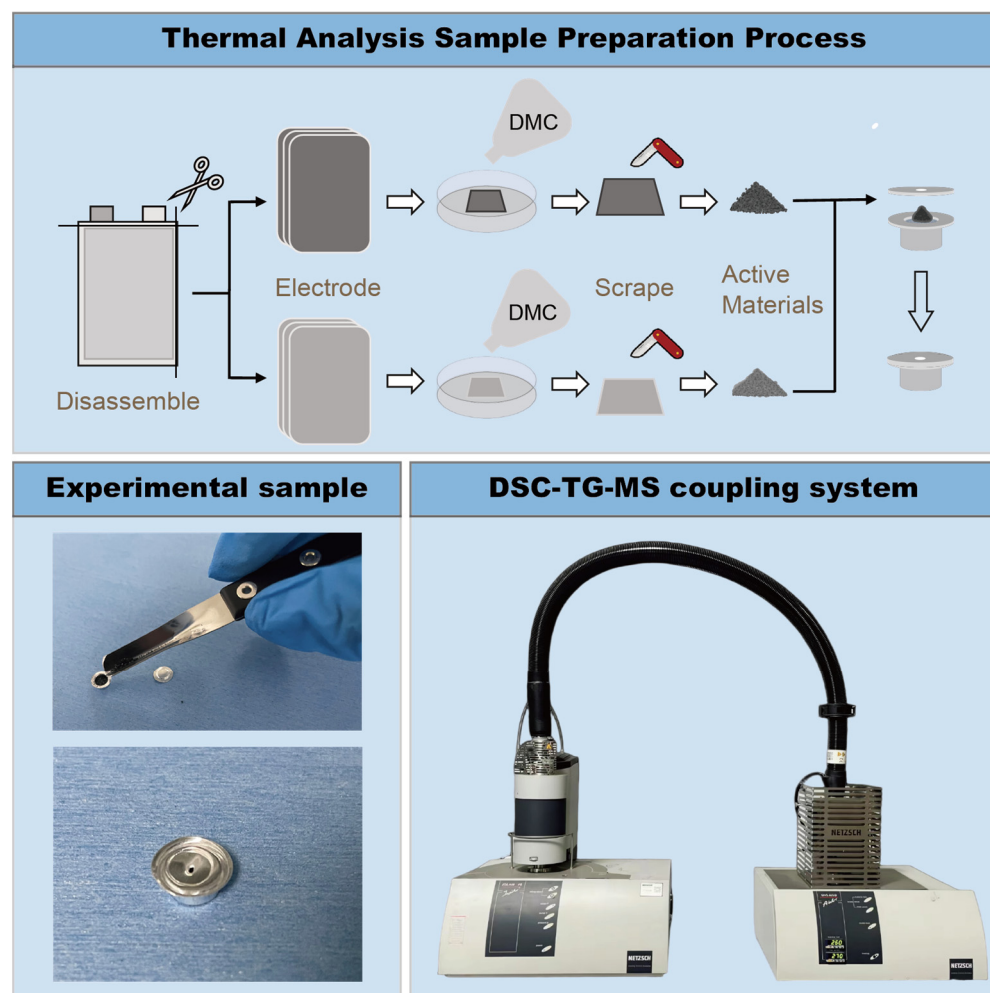


Figure 2. Process of disassembling batteries and obtaining charged samples for material thermal analysis.

Sample preparation for DSC-TG-MS tests was performed under inert atmosphere in the glove box. Single-component or mixed-component thermal analysis samples were prepared as needed, with mass ratios of cathode–anode–electrolyte consistent with those in the original cell. Electrode material powders, separators, and electrolyte were accurately weighed and loaded into standard aluminum crucibles (30 µL concave crucibles, NETZSCH-Gerätebau GmbH, Selb, Bavaria, Germany). The crucible lids were sealed using matching equipment (Figure 2). Immediately after sealing, the crucibles were quickly removed from the glove box, and a small hole was pierced at the center of the lid using a needle with diameter >0.7 mm. The crucibles were then rapidly placed into the sample cell of the DSC-TG-MS instrument (Figure 2). Finally, the required instrument parameters were set for testing. After completion, heat flow, mass loss, and gas evolution mass spectrometry signals of the electrode materials or mixed samples as a function of temperature were obtained, enabling analysis of their thermal stability and thermal failure behavior.

2.4. Characterization

The fully charged pouch disassembled in an argon-filled glove box, and the electrodes were rinsed three times with DMC and dried to obtain the fully charged cathode electrodes. As shown in Figure 3, the fully charged cathode electrode was packaged in an aluminum plastic bag in an argon-filled glove box for subsequent in situ heating XRD testing. Meanwhile, such samples were also used to undergo heating abuse to obtain material samples after thermal failure. In situ heating XRD testing was performed from 40 °C to 240 °C with a temperature step of 20 °C. The fully charged cathode electrodes were packaged in aluminum–plastic bags and heated to 200 °C using a hot box, and then the heat-failed samples were disassembled in a glove box to obtain the heat-failed electrodes and material powder. For the SEM-EDS test of cathode materials, the cathode electrode was first processed with argon ion polisher (liquid nitrogen was used to maintain the temperature at −170 °C during the treatment), and then a scanning electron microscope (SEM) (ZEISS Merlin, Carl Zeiss AG, Oberkochen, Germany) was used to observe the cross-sectional morphology and element distribution of the cathode. X-ray powder diffraction patterns were collected using a Cu source Bruker D8 ADVANCE (Bruker Corporation, Billerica, MA, USA). High-resolution TEM (HRTEM) testing was conducted with a JEM2010F (JEOL Ltd., Tokyo, Japan) transmission electron microscope.

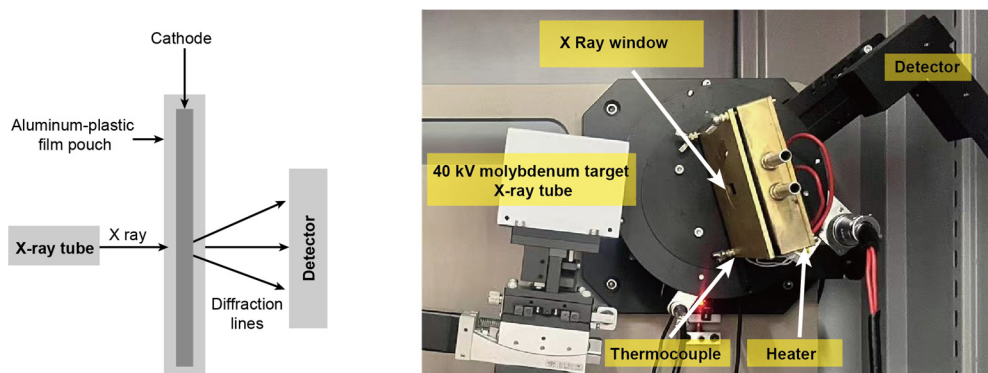


Figure 3. Schematic diagram and equipment picture of in situ heating XRD experiment.

3. Results and Discussion

3.1. Material Information and Electrochemical Performance

Lithium-rich manganese-based (LMR) cathodes ($\text{Li}_{1.2}\text{Ni}_{0.3}\text{Mn}_{0.5}\text{O}_2$) were paired with graphite anodes to assemble full cells, with detailed cell parameters provided in the Materials and Methods section. X-ray diffraction (XRD) was employed for preliminary structural characterization of the lithium-rich manganese-based cathode (Figure 4a). Rietveld refinement and crystal structure modeling revealed that the cathode consists of LiTMO_2 ($\text{TM} = \text{Ni, Mn}$) and Li_2MnO_3 phases. High-resolution transmission electron microscopy (HRTEM) images (Figure 4b) showed a distinct layered structure in the cathode, with an interplanar spacing of ~0.47 nm. Scanning electron microscopy-energy dispersive spectroscopy (SEM-EDS) was used to analyze the morphology and elemental distribution of the cathode: cross-sectional morphology indicated intact internal structures of initial particles without obvious defects or cracks (Figure 4c), while cross-sectional elemental mapping confirmed Ni and Mn as the transition metal elements in the cathode (Figure 4d). Meanwhile, the internal structure of the NCM92 cathode remains intact, and it is primarily composed of LiTMO_2 ($\text{TM} = \text{Ni, Mn}$) phases (Figure S2).

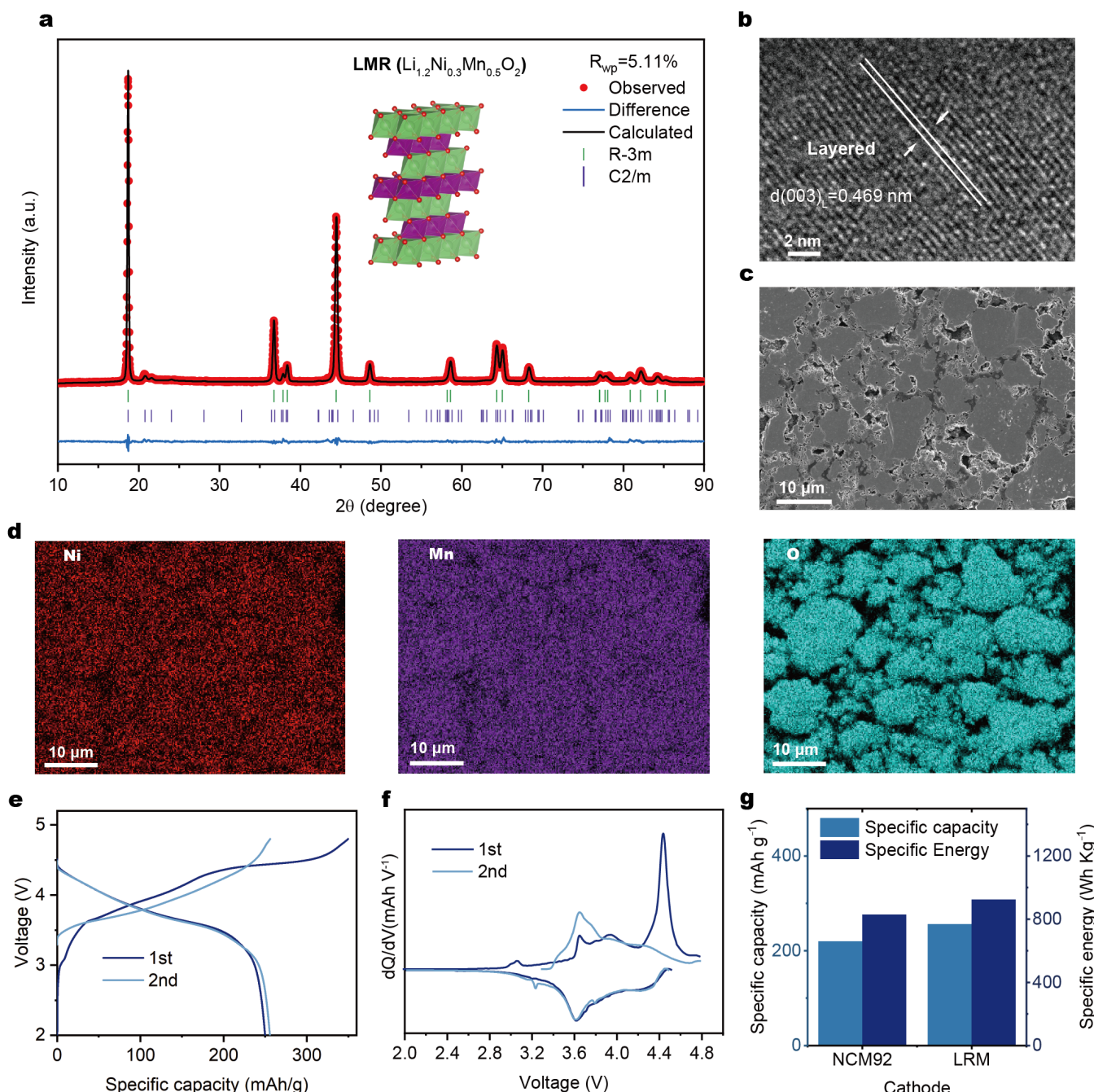


Figure 4. Lithium-rich manganese-based cathode material: (a) XRD pattern and Rietveld refinement results, (b) HRTEM image, (c) cross-sectional SEM image, and (d) elemental distribution; LMR battery: (e) first- and second-cycle voltage–capacity curves, (f) first- and second-cycle dQ/dV curves; (g) comparison of specific capacity and specific energy between LMR and NCM cathode materials.

Electrochemical tests were performed to evaluate the electrochemical performance of LMR cells. Figure 4e presents the specific capacity–voltage profiles of the first and second cycles. A prominent extended voltage plateau at ~4.5 V in the first charge profile corresponds to the activation of the lithium-rich Li_2MnO_3 phase. A sharp, intense oxidation peak near 4.5 V during the first charge cycle was also observed in the dQ/dV curve (Figure 4f), reflecting the Li_2MnO_3 activation reaction—a signature characteristic of lithium-rich cathodes. Additionally, the specific capacity and specific energy of the LMR cathode at 0.1 C were 256.0 mAh g^{-1} and 924.0 Wh Kg^{-1} , which were significantly higher than those of

the traditional high-energy nickel-rich NCM cathode (219.6 mAh g^{-1} and 829.0 Wh Kg^{-1}) (Figures 4g and S3).

3.2. Battery Safety Comparison

Accelerating rate calorimetry (ARC) tests were used to quantify battery safety. A fully charged 1 Ah LMR | Graphite cell was tested, with a fully charged 1 Ah NCM92 | Graphite cell as the control. This study focuses on the influence of material chemistry (e.g., crystal structure) on battery thermal runaway characteristics, rather than cycle-induced changes (e.g., CEI layer evolution or structural degradation); thus, the cells tested herein are fresh cells without long-term cycling. However, we recognize that long-term electrochemical cycling may alter thermal stability through surface or bulk structural changes, which constitutes a significant direction for future research. Results in Figure 5a show that compared to the LMR cell, the NCM92 cell underwent thermal runaway rapidly during testing, accompanied by a sharp temperature rise exceeding 700°C . In contrast, despite using a higher-energy-density cathode, the LMR cell exhibited a lower temperature rise rate after the onset of self-heating and experienced thermal runaway only after a nearly three times longer duration of slow self-heating. The lower temperature rise rate and extended slow self-heating period facilitate the operation of thermal management systems and provide a time window for fire-fighting intervention, reflecting the intrinsic safety of the battery.

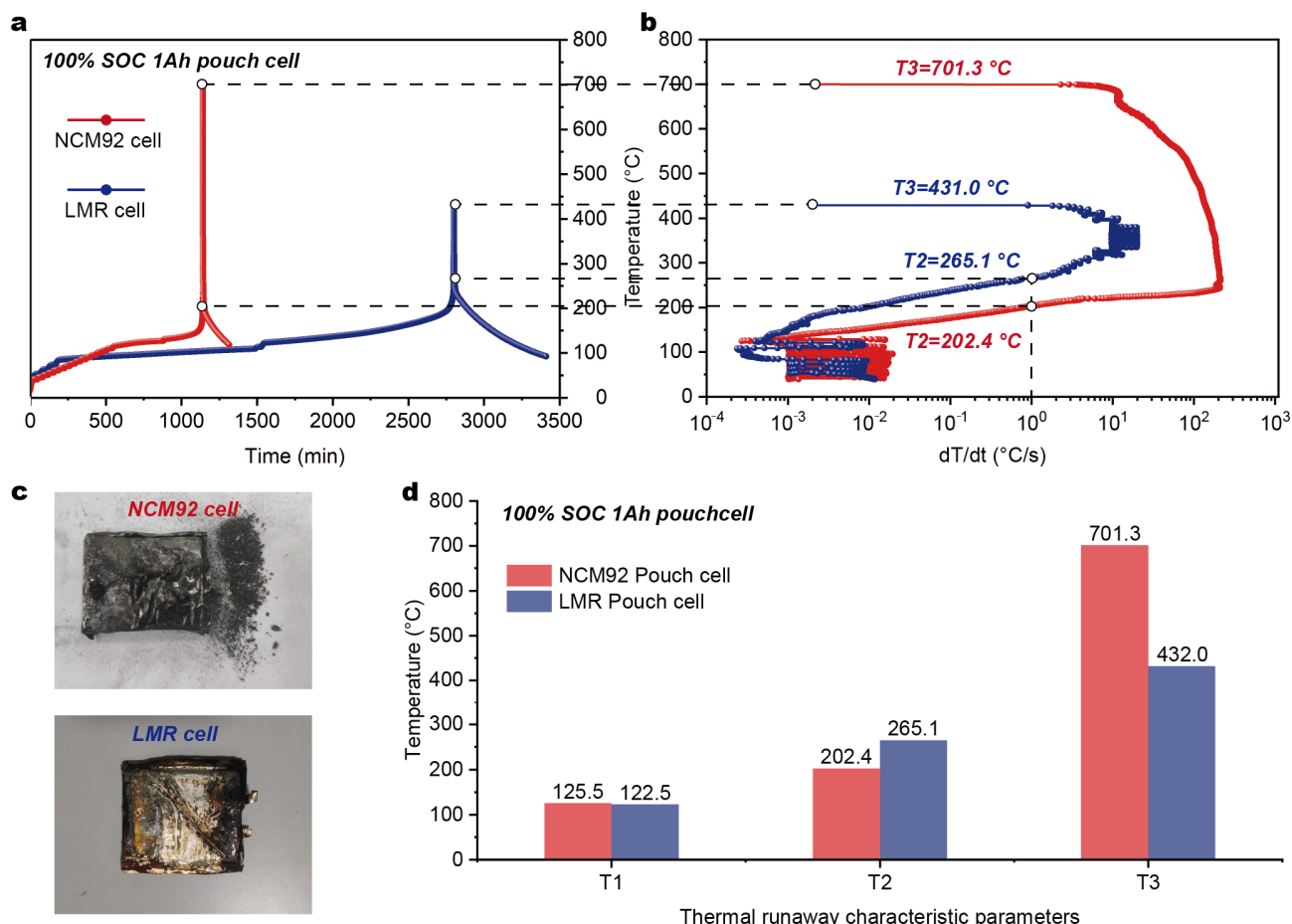


Figure 5. (a) Temperature–time curve in ARC test; (b) temperature rise rate–temperature curve in ARC test; (c) comparison of cell morphology after ARC test; (d) comparison of characteristic temperatures of two cells in ARC test.

Additionally, based on the physical significance of characteristic temperatures (Table 1), higher T1 and T2, combined with lower T3, indicate reduced thermal runaway risk and hazard, as well as higher intrinsic safety. Figure 5b shows that the LMR cell had a T2 of 256.1 °C, which is 62.7 °C higher than that of the NCM92 cell (202.4 °C), and a T3 of 431.0 °C, 270.3 °C lower than that of the NCM92 cell (701.3 °C). Images of cell residues in Figure 5c reveal severe bulging and structural damage in the NCM92 cell, indicating violent runaway and explosion during ARC testing, whereas LMR cell residues remained relatively intact with only slight bulging and no severe ejection of electrode materials—confirming their lower thermal runaway hazard.

Comparing the ARC characteristic temperatures of the two batteries: T1 values were comparable (T1 primarily depends on the thermal stability of the anode SEI), while the LMR cell showed a significantly higher T2 and a substantially lower T3 (Figure 5d). These results demonstrate that incorporating a higher-energy-density LMR cathode did not compromise the safety of lithium-ion batteries; instead, it significantly enhanced their intrinsic safety, challenging conventional understanding.

3.3. Thermal Stability of Cathode and Cathode Oxygen Release Behavior

Traditional high-energy-density Ni-rich batteries exhibit elevated thermal runaway risk due to poor cathode thermal stability and phase transitions accompanied by oxygen release at high temperatures. To address this, DSC-TG-MS was employed to analyze the thermal stability and gas release behavior of LMR cathodes. DSC results showed that the fully charged NCM92 cathode exhibits an exothermic peak at 236.8 °C with a rate of 0.96 W g⁻¹, whereas the fully charged LMR cathode shifts the exothermic peak to 290.8 °C with a reduced rate of 0.25 W g⁻¹ (Figure 6a). TG results indicate that the fully charged NCM92 cathode reaches a maximum mass loss rate of 4.40% min⁻¹ at 238.8 °C, while the fully charged LMR cathode showed a lower maximum mass loss rate of 1.10% min⁻¹ at 322.6 °C (Figure 6b). Additionally, the total mass loss of the NCM92 cathode reaches 11.87% when heated to 350 °C, compared to only 4.85% for the LMR cathode. Comparative analysis of exothermic behavior and mass loss during thermal failure confirms the superior thermal stability of LMR cathode.

Mass spectrometry (MS) coupled with DSC-TG enables *in situ* monitoring of oxygen and other oxygen-containing gas release during high-temperature cathode failure. As shown in Figure 6c, the fully charged NCM92 cathode exhibits a distinct O₂ release peak (*m/z* = 32) at 252.6 °C, whereas no significant O₂ release peak is observed for the fully charged LMR cathode—consistent with the minimal mass loss in LMR's TG profile. Under heating conditions, oxygen released from cathode materials may either be liberated as free O₂ or react with carbonaceous components in the cathode (e.g., conductive agents, binders, and other organic constituents) to form CO₂ [24]. Compared to the release of free O₂, the generation of CO₂ is more favorable for mitigating exothermic reactions within the battery [25]. As shown in Figure 6d, NCM92 cathode releases CO₂ (*m/z* = 44) at 243.5 °C, while LMR cathode exhibits an initial CO₂ peak at 199.6 °C (likely from CEI decomposition, as no significant mass loss occurs in LMR's TG curve at this stage). The main CO₂ release peak of LMR cathode appears at 297.5 °C, coinciding with its obvious mass loss. In summary, compared to NCM92, fully charged LMR cathodes not only possess better thermal stability but also release oxygen primarily as CO₂ rather than O₂, both of which help mitigate internal exothermic reactions and reduce thermal runaway risk and hazard.

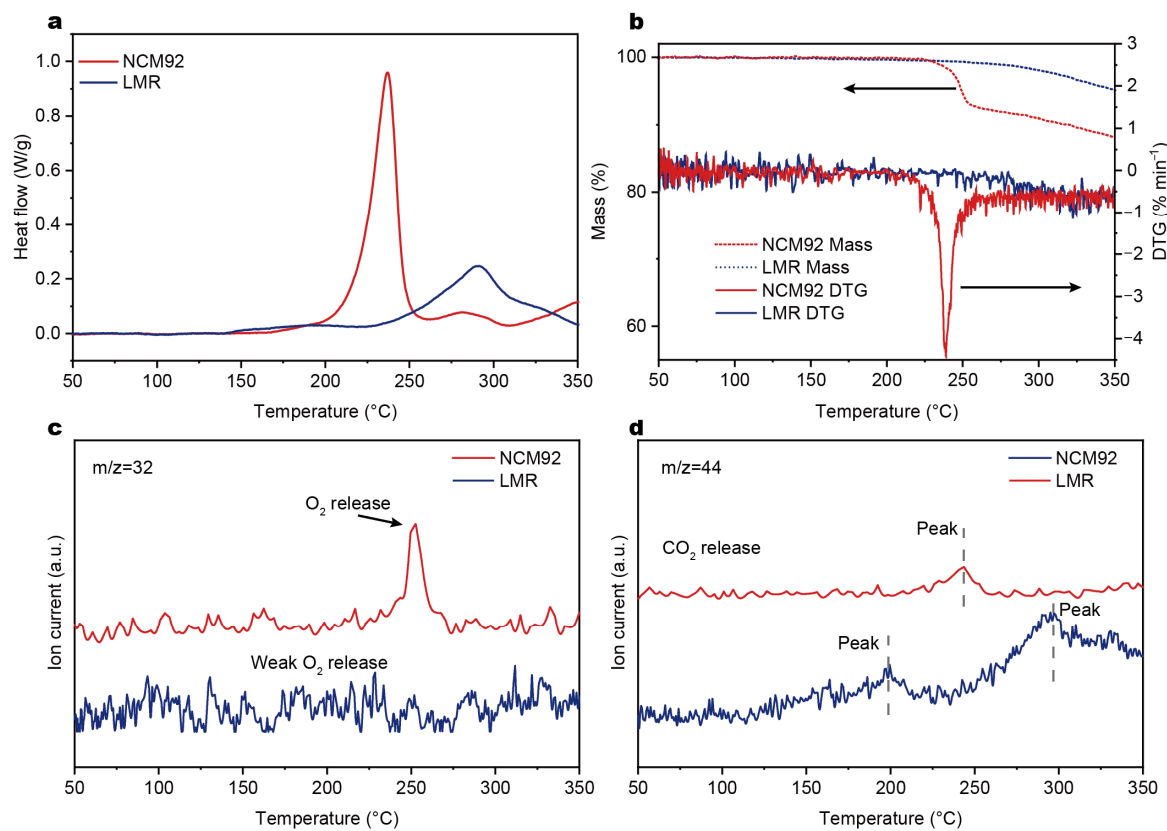


Figure 6. (a) DSC curves of the fully charged NCM92 cathode and the LMR cathode; (b) TG and DTG curves of the fully charged NCM92 cathode and the LMR cathode; MS signals of oxygen ($m/z = 32$) (c) and CO₂ ($m/z = 44$) (d) at the fully charged cathode during heating.

3.4. Structural Stability of Cathode During Heating

In situ heating XRD was employed to characterize the structural evolution of fully charged NCM92 and LMR cathodes under heating, aiming to compare the thermal stability of their crystal structures. By analyzing the diffraction peak of the layered phase-specific (003)_L plane, it was observed that when heated from 40 °C to ~170 °C, the (003)_L diffraction peak of the NCM92 cathode began to shift toward lower angles with a significant decrease in intensity—indicating the initiation of layered structure degradation (Figure 7a). In contrast, the (003)_L peak of the fully charged LMR cathode showed an obvious shift to lower 2θ values only when heated to nearly 200 °C. At 200 °C, the (003)_L peak intensity of the NCM92 cathode had weakened remarkably, while that of the LMR cathode decreased to a lesser extent, demonstrating slower degradation of the layered structure in the LMR cathode compared to NCM92 (Figure 7b).

The phase transition process was further clarified: the NCM92 cathode remained primarily in the layered phase below 172 °C, but started to transform into the spinel phase above 172 °C, forming a layered-spinel mixed phase, and completely converted to spinel phase at 207 °C (Figure 7a). For the fully charged LMR cathode, it maintained the layered phase as the dominant phase below 197 °C; the spinel phase began to emerge with further heating, but even at 240 °C, the transition to the spinel phase was incomplete (Figure 7b). Overall, in situ heating XRD results confirm that fully charged LMR cathodes exhibit higher structural thermal stability than NCM92 cathodes.

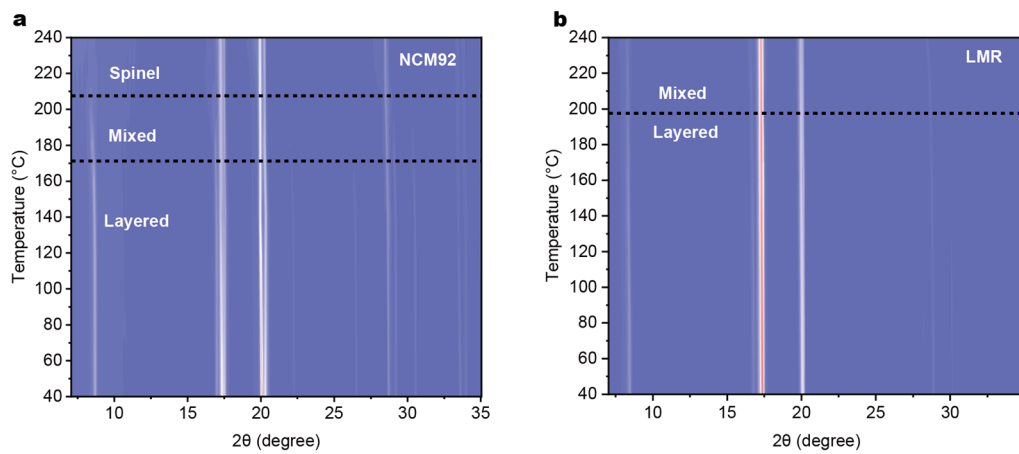


Figure 7. In situ heating XRD results of (a) fully charged NCM92 cathode and (b) fully charged LMR cathode.

3.5. Structural Degradation of Cathode After Thermal Abuse

To further verify the thermal stability of fully charged LMR cathodes, high-resolution transmission electron microscopy (HRTEM) was performed on fully charged NCM92 and LMR cathodes before and after 200 °C thermal abuse, aiming to analyze the degradation degree of their crystal structures after thermal failure. HRTEM images show that the fully charged NCM92 cathode primarily consists of a layered structure before thermal abuse (Figure 8a). After 200 °C thermal abuse, however, both the edge and bulk phases of the NCM92 cathode significantly degraded into spinel phase (Figure 8b), consistent with the in situ heating XRD results, confirming severe degradation of the layered structure in fully charged NCM92 cathode at 200 °C.

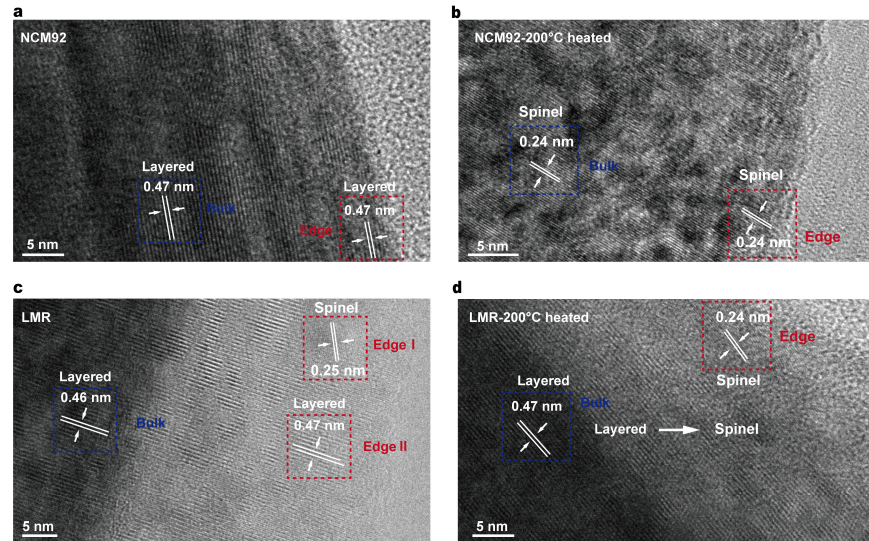


Figure 8. HRTEM images of the fully charged NCM92 cathode before thermal abuse (a) and after thermal abuse at 200 °C (b); HRTEM images of the fully charged LMR cathode before thermal abuse (c) and after thermal abuse at 200 °C (d).

In contrast, the fully charged LMR cathode mainly exhibits a layered structure before thermal abuse, with only a small amount of dispersed spinel phase at the material edge—likely representing surface degradation induced by high-voltage cycling (Figure 8c). After 200 °C thermal abuse, a continuous spinel phase forms at the edge of LMR cathode, accompanied by a layered-spinel mixed transition zone, while the bulk phase retains the

layered structure (Figure 8d). Collectively, these results confirm that fully charged LMR cathodes exhibit superior structural thermal stability compared to NCM92 cathodes.

3.6. Exothermic Behavior of Full-Cell Material-Level Reactions

To further analyze the influence of cathode materials on internal exothermic reactions in batteries, DSC was employed for material-level thermal testing of mixed samples (fully charged cathodes with electrolyte) and full-cell samples. DSC results showed that compared to the main exothermic reactions in the NCM92-cathode electrolyte sample, those in the LMR-cathode electrolyte sample occurred at higher temperature with a lower exothermic rate (Figure S1). DSC results for full-cell samples revealed that the full-cell sample with the NCM92 cathode exhibited the first exothermic peak at $190.1\text{ }^{\circ}\text{C}$ with a rate of 0.86 W g^{-1} , whereas the full-cell sample with the LMR cathode showed its first exothermic peak at $207.0\text{ }^{\circ}\text{C}$, with a lower rate of 0.58 W g^{-1} (Figure 9).

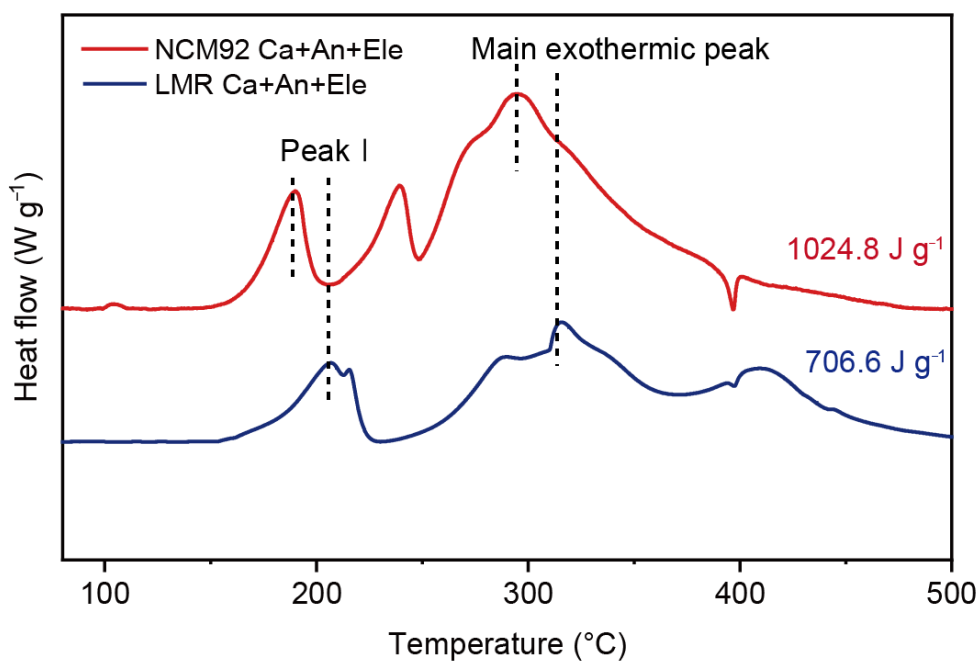


Figure 9. DSC curves of NCM92 and LMR full-cell DSC samples.

Additionally, the main exothermic reaction of the NCM92 full-cell sample occurred at $295.4\text{ }^{\circ}\text{C}$ with a rate of 1.57 W g^{-1} , while the main exothermic peak of the LMR full-cell sample appeared at $316.3\text{ }^{\circ}\text{C}$ with a rate of 0.87 W g^{-1} (Figure 9). Collectively, the temperature shift and attenuated heat flow at both reaction stages demonstrate that despite its higher specific capacity and energy density, the LMR cathode possesses superior thermal stability and lower reactivity than NCM92. This translates to a 31% reduction in total heat generation for the LMR full-cell sample (Figure 9), confirming its role in mitigating internal exothermic reactions.

4. Conclusions

In conclusion, systematic comparative analyses reveal that the application of higher-energy-density lithium-rich manganese-based (LMR) cathodes significantly reduces the thermal runaway risk and hazard of batteries, challenging the conventional notion that high-energy cathodes inevitably compromise battery safety. Material-level thermal analyses demonstrate that fully charged LMR cathodes exhibit superior thermal stability compared to NCM92 cathodes. Additionally, mass spectrometry results confirm that LMR cathodes release negligible O_2 during high-temperature failure, with oxygen primarily evolving as

CO_2 . This difference in cathode oxygen release behavior helps mitigate internal exothermic reactions, reducing thermal runaway risks.

Furthermore, *in situ* heating XRD and HRTEM analyses clarify the high-temperature structural stability of fully charged cathodes: NCM92 cathodes begin transforming from layered to spinel phases at 172 °C, fully converting to spinel by 207 °C; in contrast, LMR cathodes only start forming spinel phases at 197 °C and remain incompletely transformed even at 240 °C. Microstructural observations after 200 °C thermal abuse further confirm that NCM92 cathodes almost fully convert to spinel, while LMR cathodes retain intact layered structures in their bulk phases—confirming superior high-temperature structural stability. This stability shifts the exothermic peaks of the LMR full-cell DSC sample to higher temperatures with lower rates, reducing the total exothermic heat by 31% and significantly enhancing intrinsic battery safety.

This study resolves the trade-off between high-energy cathode application and battery safety, highlights thermal stability and cathode oxygen release behavior as critical metrics for evaluating the safety of new cathodes, and provides guidance for developing high-energy cathodes. These findings enable the practical application of high-energy-density, high-safety batteries.

Supplementary Materials: The following supporting information can be downloaded at <https://www.mdpi.com/article/10.3390/batteries11080311/s1>; Figure S1: Heat flow curves of the reaction between the fully charged NCM cathode and the electrolyte and the LMR cathode and the electrolyte. Figure S2: NCM92 cathode material: (a) XRD pattern and Rietveld refinement results, (b) cross-sectional SEM image, (c) cross-sectional element distribution. Figure S3: LMR battery: (a) first and second cycle voltage-capacity curves, (b) first and second cycle dQ/dV curves.

Author Contributions: Conceptualization, Z.P. and X.F.; methodology, Y.W.; software, S.F.; validation, Z.P., Y.W. and S.F.; formal analysis, Z.H. and L.W.; investigation, Z.W.; resources, X.F., L.W. and X.H.; data curation, C.X.; writing—original draft preparation, Z.P.; writing—review and editing, L.W. and X.H.; visualization, Z.P. and C.X.; supervision, L.W. and X.H.; project administration, X.F. and Y.W.; funding acquisition, X.F. All authors have read and agreed to the published version of the manuscript.

Funding: This research was funded by the National Key R&D Program-Strategic Scientific and Technological Innovation Cooperation (Grant No. 2022YFE0207900); the National Key R&D Program-Strategic Scientific and Technological Innovation Cooperation (Grant No. 2022YFB2404400); the National Natural Science Foundation of China (Grant No. 51706117, Grant No. 52076121, Grant No. 52406256, Grant No. 22279070, Grant No. U21A20170, Grant No. 52422609 and Grant No. 52406256); and the Independent Research Project of the State Key Laboratory of Intelligent Green Vehicle and Mobility, Tsinghua University (Grant No. ZZ-PY-20250109).

Data Availability Statement: The data that support the findings of this study are available from the corresponding author upon reasonable request.

Acknowledgments: These authors contributed equally: Zhaoqiang Pei, Shaobo Feng. We would like to show gratitude to the Beijing Natural Science Foundation (L242005).

Conflicts of Interest: The authors declare no conflict of interest.

References

1. Tarascon, J.-M.; Armand, M. Issues and Challenges Facing Rechargeable Lithium Batteries. *Nature* **2001**, *414*, 359–367. [[CrossRef](#)]
2. Ji, H.; Wu, J.; Cai, Z.; Liu, J.; Kwon, D.-H.; Kim, H.; Urban, A.; Papp, J.K.; Foley, E.; Tian, Y.; et al. Ultrahigh Power and Energy Density in Partially Ordered Lithium-Ion Cathode Materials. *Nat. Energy* **2020**, *5*, 213–221. [[CrossRef](#)]
3. Lee, W.; Muhammad, S.; Sergey, C.; Lee, H.; Yoon, J.; Kang, Y.-M.; Yoon, W.-S. Advances in the Cathode Materials for Lithium Rechargeable Batteries. *Angew. Chem. Int. Ed.* **2020**, *59*, 2578–2605. [[CrossRef](#)]

4. Li, Q.; Zhou, D.; Chu, M.; Liu, Z.; Yang, L.; Wu, W.; Ning, D.; Li, W.; Liu, X.; Li, J.; et al. A Comprehensive Understanding on the Anionic Redox Chemistry of High-Voltage Cathode Materials for High-Energy-Density Lithium-Ion Batteries. *Chem. Soc. Rev.* **2025**, *54*, 3441–3474. [[CrossRef](#)] [[PubMed](#)]
5. Luo, D.; Zhu, H.; Xia, Y.; Yin, Z.; Qin, Y.; Li, T.; Zhang, Q.; Gu, L.; Peng, Y.; Zhang, J.; et al. A Li-Rich Layered Oxide Cathode with Negligible Voltage Decay. *Nat. Energy* **2023**, *8*, 1078–1087. [[CrossRef](#)]
6. Feng, X.; Ren, D.; He, X.; Ouyang, M. Mitigating Thermal Runaway of Lithium-Ion Batteries. *Joule* **2020**, *4*, 743–770. [[CrossRef](#)]
7. Deng, Z.; Liu, Y.; Wang, L.; Fu, N.; Li, Y.; Luo, Y.; Wang, J.; Xiao, X.; Wang, X.; Yang, X.; et al. Challenges of Thermal Stability of High-Energy Layered Oxide Cathode Materials for Lithium-Ion Batteries: A Review. *Mater. Today* **2023**, *69*, 236–261. [[CrossRef](#)]
8. Meng, J.; Qu, G.; Huang, Y. Stabilization Strategies for High-Capacity NCM Materials Targeting for Safety and Durability Improvements. *eTransportation* **2023**, *16*, 100233. [[CrossRef](#)]
9. Li, J.; Gao, P.; Tong, B.; Cheng, Z.; Cao, M.; Mei, W.; Wang, Q.; Sun, J.; Qin, P. Revealing the Mechanism of Pack Ceiling Failure Induced by Thermal Runaway in NCM Batteries: A Coupled Multiphase Fluid-Structure Interaction Model for Electric Vehicles. *eTransportation* **2024**, *20*, 100335. [[CrossRef](#)]
10. He, M.; Chartouni, D.; Landmann, D.; Colombi, S. Safety Aspects of Stationary Battery Energy Storage Systems. *Batteries* **2024**, *10*, 418. [[CrossRef](#)]
11. Liu, X.; Ren, D.; Hsu, H.; Feng, X.; Xu, G.-L.; Zhuang, M.; Gao, H.; Lu, L.; Han, X.; Chu, Z.; et al. Thermal Runaway of Lithium-Ion Batteries without Internal Short Circuit. *Joule* **2018**, *2*, 2047–2064. [[CrossRef](#)]
12. Wang, Y.; Feng, X.; Huang, W.; He, X.; Wang, L.; Ouyang, M. Challenges and Opportunities to Mitigate the Catastrophic Thermal Runaway of High-Energy Batteries. *Adv. Energy Mater.* **2023**, *13*, 2203841. [[CrossRef](#)]
13. Li, Y.; Liu, X.; Wang, L.; Feng, X.; Ren, D.; Wu, Y.; Xu, G.; Lu, L.; Hou, J.; Zhang, W.; et al. Thermal Runaway Mechanism of Lithium-Ion Battery with $\text{LiNi}_{0.8}\text{Mn}_{0.1}\text{Co}_{0.1}\text{O}_2$ Cathode Materials. *Nano Energy* **2021**, *85*, 105878. [[CrossRef](#)]
14. Shi, C.; Wang, H.; Shen, H.; Wang, J.; Li, C.; Li, Y.; Xu, W.; Li, M. Thermal Runaway Characteristics and Gas Analysis of $\text{LiNi}_{0.9}\text{Co}_{0.05}\text{Mn}_{0.05}\text{O}_2$ Batteries. *Batteries* **2024**, *10*, 84. [[CrossRef](#)]
15. Cui, Z.; Liu, C.; Wang, F.; Manthiram, A. Navigating Thermal Stability Intricacies of High-Nickel Cathodes for High-Energy Lithium Batteries. *Nat. Energy* **2025**, *10*, 490–501. [[CrossRef](#)]
16. Li, K.; Wang, L.; Wang, Y.; Feng, X.; Jiang, F.; Ouyang, M. Correlating Phase Transition with Heat Generation through Calorimetric Data. *eScience* **2024**, *4*, 100226. [[CrossRef](#)]
17. Sun, Y.; Ren, D.; Liu, G.; Mu, D.; Wang, L.; Wu, B.; Liu, J.; Wu, N.; He, X. Correlation between Thermal Stabilities of Nickel-Rich Cathode Materials and Battery Thermal Runaway. *Int. J. Energy Res.* **2021**, *45*, 20867–20877. [[CrossRef](#)]
18. Liu, T.; Liu, J.; Li, L.; Yu, L.; Diao, J.; Zhou, T.; Li, S.; Dai, A.; Zhao, W.; Xu, S.; et al. Origin of Structural Degradation in Li-Rich Layered Oxide Cathode. *Nature* **2022**, *606*, 305–312. [[CrossRef](#)]
19. Jin, Y.; Zhao, Z.; Ren, P.-G.; Zhang, B.; Chen, Z.; Guo, Z.; Ren, F.; Sun, Z.; Liu, S.; Song, P.; et al. Recent Advances in Oxygen Redox Activity of Lithium-Rich Manganese-Based Layered Oxides Cathode Materials: Mechanism, Challenges and Strategies (Adv. Energy Mater. 40/2024). *Adv. Energy Mater.* **2024**, *14*, 2470173. [[CrossRef](#)]
20. Zhang, X.; Wang, B.; Zhao, S.; Li, H.; Yu, H. Oxygen Anionic Redox Activated High-Energy Cathodes: Status and Prospects. *eTransportation* **2021**, *8*, 100118. [[CrossRef](#)]
21. Hua, W.; Wang, S.; Knapp, M.; Leake, S.J.; Senyshyn, A.; Richter, C.; Yavuz, M.; Binder, J.R.; Grey, C.P.; Ehrenberg, H.; et al. Structural Insights into the Formation and Voltage Degradation of Lithium- and Manganese-Rich Layered Oxides. *Nat. Commun.* **2019**, *10*, 5365. [[CrossRef](#)] [[PubMed](#)]
22. Shen, C.; Hu, L.; Duan, Q.; Liu, X.; Huang, S.; Jiang, Y.; Li, W.; Zhao, B.; Sun, X.; Zhang, J. Understanding Lattice Oxygen Redox Behavior in Lithium-Rich Manganese-Based Layered Oxides for Lithium-Ion and Lithium-Metal Batteries from Reaction Mechanisms to Regulation Strategies. *Adv. Energy Mater.* **2023**, *13*, 2302957. [[CrossRef](#)]
23. Ohneseit, S.; Finster, P.; Floras, C.; Lubenau, N.; Uhlmann, N.; Seifert, H.J.; Ziebert, C. Thermal and Mechanical Safety Assessment of Type 21700 Lithium-Ion Batteries with NMC, NCA and LFP Cathodes—Investigation of Cell Abuse by Means of Accelerating Rate Calorimetry (ARC). *Batteries* **2023**, *9*, 237. [[CrossRef](#)]
24. Xia, X.; Dahn, J.R. A Study of the Reactivity of De-Intercalated $\text{NaNi}_{0.5}\text{Mn}_{0.5}\text{O}_2$ with Non-Aqueous Solvent and Electrolyte by Accelerating Rate Calorimetry. *J. Electrochem. Soc.* **2012**, *159*, A1048. [[CrossRef](#)]
25. Li, Q.; Li, Y.; Liu, M.; Li, Y.; Zhao, H.; Ren, H.; Zhao, Y.; Zhou, Q.; Feng, X.; Shi, J.; et al. Elucidating Thermal Decomposition Kinetic Mechanism of Charged Layered Oxide Cathode for Sodium-Ion Batteries. *Adv. Mater.* **2025**, *37*, 2415610. [[CrossRef](#)] [[PubMed](#)]

Disclaimer/Publisher’s Note: The statements, opinions and data contained in all publications are solely those of the individual author(s) and contributor(s) and not of MDPI and/or the editor(s). MDPI and/or the editor(s) disclaim responsibility for any injury to people or property resulting from any ideas, methods, instructions or products referred to in the content.